How to cite: Angew. Chem. Int. Ed. 2024, e202402522
doi.org/10.1002/anie.202402522

Immunotherapy

Cancer Cell-Selective PD-L1 Inhibition via a DNA Safety Catch to Enhance Immunotherapy Specificity

*Shiyi Bi, Wei Chen, Yanyun Fang, Jieyu Shen, Qing Zhang, Hongqian Guo, Huangxian Ju, and Ying Liu**

Abstract: Immune checkpoint protein blockade (ICB) has emerged as a powerful immunotherapy approach, but suppressing immune-related adverse events (irAEs) for noncancerous cells and normal tissues remains challenging. Activatable ICB has been developed with tumor microenvironment highly-expressed molecules as stimuli, but they still lack precision and efficiency considering the diffusion of stimuli molecules in whole tumor tissue. Here we assemble PD–L1 with a duplex DNA strand, termed as "safety catch", to regulate its accessibility for ICB. The safety catch remains at "on" status for noncancerous cells to prevent ICB binding to PD–L1. Cancer cell membrane protein c-Met acts as a trigger protein to react with safety catch, which selectively exposes its hybridization region for ICB reagent. The ICB reagent is a retractable DNA nanostring with repeating hairpin-structural units, whose contraction drives PD–L1 clustering with endocytosis-guided degradation. The safety catch, even remained at "safety on" status, is removed from the cell membrane via a DNA strand displacement reaction to minimize its influence on noncancerous cells. This strategy demonstrates selective and potent immunotherapeutic capabilities only against cancer cells both in vitro and in vivo, and shows effective suppression of irAEs in normal tissues, therefore would become a promising approach for precise immunotherapy in mice.

[*] S. Bi, Y. Fang, J. Shen, Prof. H. Ju, Prof. Y. Liu
State Key Laboratory of Analytical Chemistry for Life Science
School of Chemistry and Chemical Engineering, Nanjing University
Nanjing 210023, China
E-mail: yingliu@nju.edu.cn

W. Chen, Dr. Q. Zhang, Prof. H. Guo
Department of Urology
Affiliated Drum Tower Hospital,
Medical School of Nanjing University
Institute of Urology, Nanjing University
Nanjing 210008, China

Prof. Y. Liu
Chemistry and Biomedicine Innovation Center
Nanjing University
Nanjing 210023, China

Introduction

As a promising immunotherapy strategy, immune checkpoint blockade (ICB) has a durable and broad impact on numerous types of tumors.[1] The connections of immune checkpoint proteins (ICP) with their partner proteins prevent immune system activation, and immune checkpoint inhibitors block these connections to boost immune response in ICB strategy.[2] Programmed cell death protein 1 (PD1)/programmed-death ligand 1 (PD–L1) are the most common ICPs,[3] PD1 is highly expressed in tumor-infiltrating T cells, PD–L1 is expressed by tumor cells and other cell types including endothelial cells, epithelial cells, and myeloid cells. Their interaction could be blocked either by inhibiting PD1 for T cells or by inhibiting PD–L1 for tumor cells, which both enhance the antitumor response of T cells,[4] The corresponding inhibitors include small-molecule drugs,[5] DNA,[6] peptides,[7] and antibodies.[8]

Current ICB strategies mainly focus on developing ICB reagent delivery strategy, adjusting tumor microenvironment and remodeling immune cells, which have won success with progressive implementation in clinical practice.[9] However, the nonselective inhibition of immune checkpoint proteins for all cell types would make the immune system indiscriminately attack cancer cells and noncancerous cells. The corresponding immune-related adverse events (irAEs) have emerged as a key challenge.[10] Take PD–L1 as an example, in addition to cancer cells, it is also expressed on antigen-presenting cells and nonlymphoid tissues, including heart, lung, and islet,[11] to avoid normal tissue damage. Currently reported PD–L1 inhibition strategies generally lack activation control with cancer cell selectivity, which would impair inhibition efficiency and result in the occurrence of irAEs with 'on-target, off-tumor' cytotoxicity[12] including gastrointestinal damage,[13] diabetes[14] and rheumatoid arthritis.[15] Therefore, developing a selective ICB strategy that is active only against cancer cells but not normal organs is urgently needed.

Direct degradation of ICPs via cross-linking guided endocytosis is a promising ICB strategy with improved operation controllability.[16] Taking tumor microenvironment highly expressed molecules, such as glutathione (GSH),[17] alkaline phosphatase (ALP)[18] as stimuli, responsive peptides assembly[19] strategies have been developed to regulate ICPs clustering and degradation via lysosomal pathway. However, these microenvironment-relied manipulation strategies still lack selectivity at the cellular level. Naturally developed solid tumors possess complex tissue composition

which contains not only cancer cells but also adjacent normal cells such as immune cells and normal fibroblasts that also express ICPs.[20] The above-mentioned microenvironment stimuli molecules are widely distributed in whole tumor tissue and even diffuse to systemic circulation,[21] which would impair regulation precision and decrease the therapeutic result of ICB strategy.

Compared with regulating ICP cross-linking process with the above-mentioned "movable" stimuli molecules,[19] directly endowing cancer cell and normal cell ICPs with different accessibilities for ICB reagents would be more efficient and provide selectivity at the cellular level. Cancer cell membrane is the natural barrier to distinguish them from normal cells and is decorated with distinct membrane receptor proteins, such as cell-mesenchymal epithelial transforming factor (c-Met),[22] HER-2[23] and PSMA,[24] which can work as "membrane-embedded" stimuli to manipulate the accessibility of ICP for ICB reagents. Herein, we refit PD–L1 with a "safety catch" DNA strand, which remains at "safety-on" status for noncancerous cells and inhibits the accessibility of PD–L1 to ICB reagent. Cancer cell membrane protein c-Met acts as the activation trigger to convert safety catch DNA strand to "safety-off" status and recovers the accessibility of PD–L1 to ICB reagent. Through manipulating "on/off" status of safety catch, PD–L1 degradation is secured selectively for cancer cells with little effect on normal cells. A duplex-structured DNA strand PL-PC is assembled on PD–L1 to act as a safety catch, and a DNA nanostring (DNS) is used as an ICB reagent to cluster PD–L1 on cell membrane for PD–L1 endocytosis and degradation. The DNS recognition region on PL was sealed by hybridization with PC (Scheme 1A, Safety catch PL-PC), which keeps safety-catch PL-PC at "safety on" status and prevents the anchoring of DNS on cell membrane for normal cells (Scheme 1A, Normal cell). MH_{DBCO}, a hairpin-structured DNA that contains c-Met recognition sequence and 3' terminus DBCO labeling, is anchored to azide labeled c-Met and fixed via simultaneous click chemistry. Recognition of c-Met exposes PC hybridization region on MH_{DBCO}, which acts as the trigger for safety catch status conversion. The encountering of c-Met and PD–L1 initiates a strand displacement reaction between MH_{DBCO} and PL-PC, which forms MH_{DBCO}-PC duplex and converts safety catch to "safety off" status with the exposure of DNS recognition region on PL (Scheme 1A, Cancer cell). The major function of safety catch is to selectively protect normal cells "safe" from DNS binding.

To generate DNS, a retractable DNA scaffold (DSC) is synthesized via rolling circle amplification (RCA), and hybridizes with H2 strand to fix the "extended" configuration. SRL_{DBCO}-RC duplex strand is also hybridized with DSC, which subsequently reacts with PL ("safety off" status) via strand displacement reaction to anchor DNS to PD–L1 (Scheme 1B, DNS). DNS is added after anchoring safety catch PL-PC on both cancer cell and normal cell surface. PD–L1 is also labeled with azide, which further fastens DNS via click reaction with DBCO that is labeled on SRL_{DBCO}-RC. The contraction of DNS is performed by the addition of DNA strand H1, which pulls H2 off from DNS by generating H1-H2 duplex and results in PD–L1 aggregation and degradation via lysosomal pathway (Scheme 1B, Cancer cell). On the contrary, DNS could not anchor to normal cells with PL-PC safety catch remaining at "safety-on" status, which protects normal cells against systematic toxicity. After the selective anchoring of DNS to cancer cells, it is necessary to erase safety catch PL-PC from PD–L1 to completely suppress irAEs and eliminate influence on physiologic function of normal cells. Therefore, eraser strand LP is added after DNS binding process. LP has a higher affinity to PL and completely removes safety catch from PD–L1 by forming PL-LP duplex structure (Scheme 1B, Normal cell). The removal of PL from cancer cell membrane doesn't affect anchored DNS since it is click-fastened on cancer cell membrane. The safety catch secures efficient and cancer cell-selective PD–L1 clearance with effective suppression of irAEs, therefore would be beneficial to immunotherapy.

Results and Discussion

Synthesis and Structure Conversion of DNS

As the skeleton for DNS, DSC was produced by rolling circle amplification (RCA) reaction. The successful generation of DSC demonstrated a new band with the least mobility on polyacrylamide gel electrophoresis (PAGE) (Figure S1A, lane 6) due to its large molecular mass and size.[25] DSC was then alternately hybridized with DNA strands H2 and SRL-RC to obtain DNS. A stretchable region was contained in DSC, which hybridized with H2 and formed rigid double-stranded structure with the dispersed location of SRL-RC (Figure 1A, DNS). DNS correspondingly demonstrated a rigid linear structure on AFM image (Figure 1B). DNA strand H1 hybridized with H2 via strand displacement reaction, which recovered the hairpin structure of stretchable region on DSC and shortened the space among SRL-RCs (Figure 1A). Half-completed DNS (H-DNS) (Figure 1C, lane 4) was obtained by annealing DSC (Figure 1C, lane 1) and H2 (Figure 1C, lane 3), and used instead of DNS to simplify structure change characterization process. The configuration change of H-DNS was controlled via the binding and release of H2 and confirmed via PAGE analysis. Mixing H-DNS with H1 showed the complete disappearance of H1 band in accompany with the appearance of the H1-H2 duplex bands (Figure 1C, lane 5), indicating the detachment of H2 and corresponding recovery of hairpin structure in stretchable region of H-DNS. To clearly show structure/molecular difference of H-DNS before and after the detachment of H2, DNA strand H with a single RCA repeating sequence was synthesized (Figure S1B, lane 1) and hybridized with H2 (Figure S1B, lane 3) to obtain H–H2 duplex strand with a lower mobility in PAGE (Figure S1B, lane 4). H–H2 showed a similar reaction result as that of H-DNS. H–H2 mixing with H1 generated H1-H2 duplex band, and H band with the disappearance of H1 band (Figure S1B, lane 5).

To further verify the structure conversion between DSC and H-DNS, TAMRA-labelled DNA strand S1 ($S1_T$) and

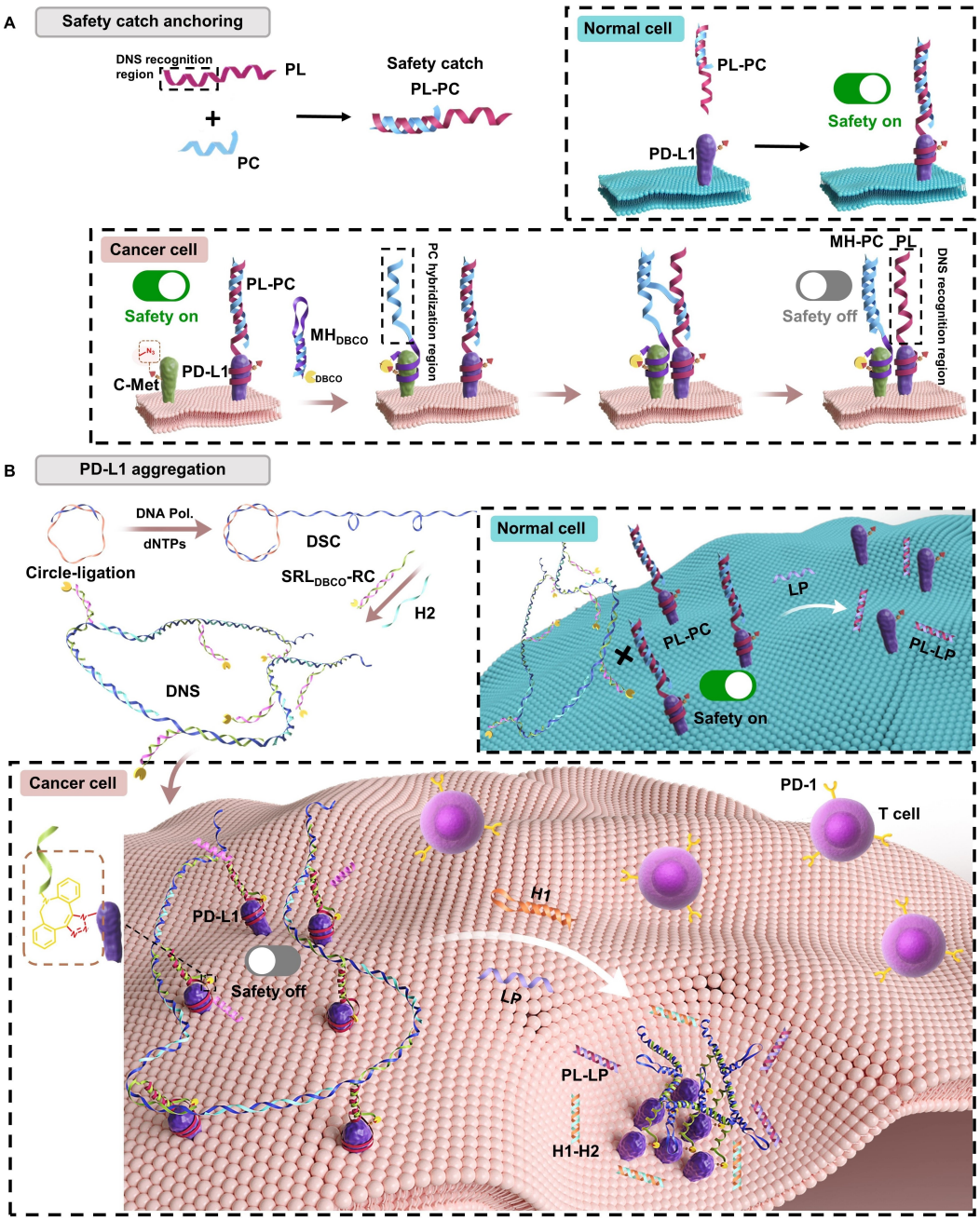

Scheme 1. Schematic illustration of the "safety catch" anchored PD–L1 for cancer cell-selective PD–L1 degradation. (A) The synthesis of safety catch PL-PC and c-Met regulated status conversion of safety catch for cancer/normal cells. Safety catch PL-PC is prepared by PL/PC hybridization and binds to PD–L1 for both cancer cells and normal cells. With DNS recognition region sealed, PL-PC remained at "safety on" status at this stage. MH_{DBCO}, a hairpin-structure DNA containing c-Met recognition region, binds to c-Met for cancer cells and exposes PC hybridization region, which then reacts with PL-PC via a strand displacement reaction to convert safety catch PL-PC to "safety off" status (PL). For normal cells, the safety catch PL-PC remains at "safety on" status with the absence of c-Met. (B) DNS synthesis and application for contraction-triggered PD–L1 degradation to boost T cell activity. DSC with repeating hairpin units is synthesized via RCA. DSC is alternatively hybridized with H2 and SRL_{DBCO}-RC duplex strand to generate DNS. H2 strand fixes the DNS in an "extended" configuration, SRL_{DBCO}-RC duplex strand acts as an anchor to bind DNS to cell membrane via a strand displacement reaction with DNS recognition region ("safety off" status, PL). DNA strand H1 is subsequently added to pull H2 off from DNS, which results in PD–L1 aggregation and degradation via lysosomal pathway. Normal cells are not accessible for DNS binding with PL-PC remained at "safety on" status. Eraser strand, LP, is then added to remove safety catch PL-PC from both cells.

BHQ2-labelled DNA strand S3 ($S3_B$) were hybridized with DSC to obtain $DSC_{T/B}$ (Figure S2A). The stretchable region kept hairpin structure in DSC, therefore TAMRA and BHQ2 were located in proximity and generated little TAMRA fluorescence (Figure S2B, $DSC_{T/B}$). Reacting with H2 stretched $DSC_{T/B}$ to H-$DNS_{T/B}$, which extended the distance between TAMRA and BHQ2 and increased TAMRA fluorescence by ~25 times (Figure S2B, H-$DNS_{T/}$

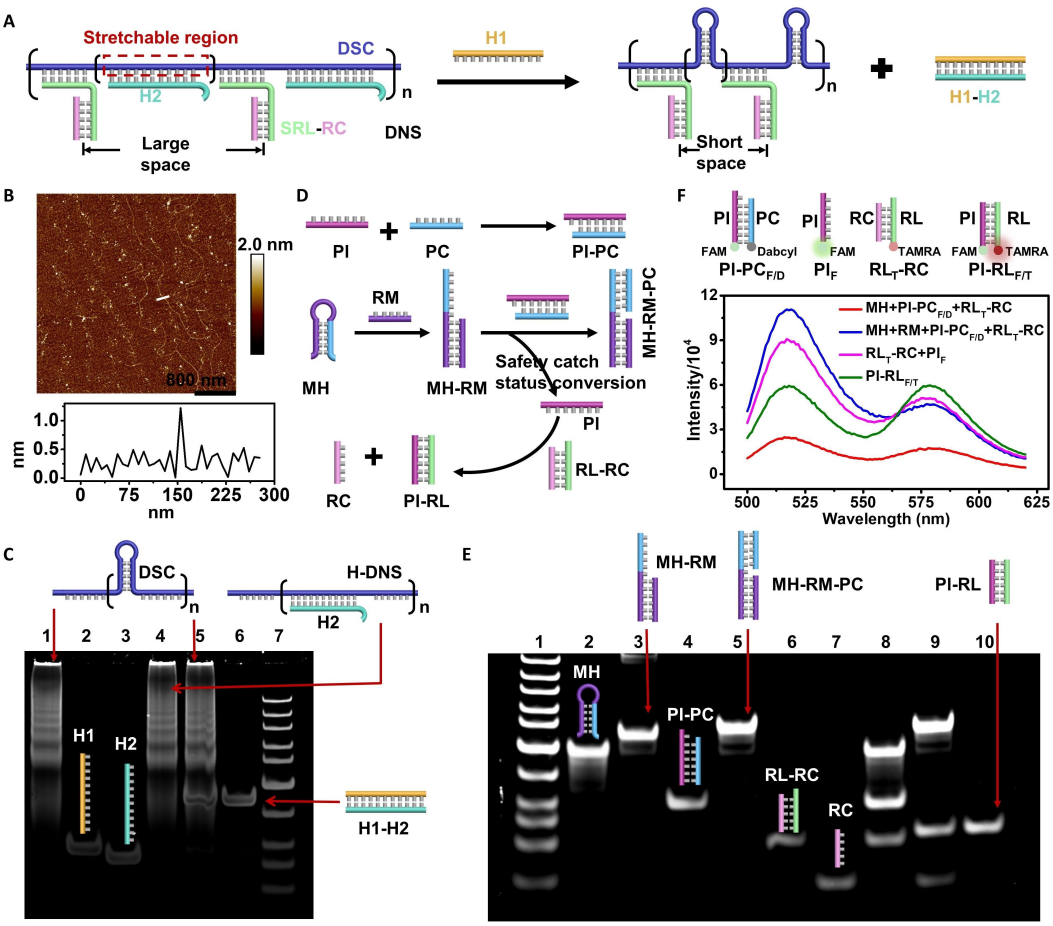

Figure 1. The synthesis and structural conversion of DNS. (A) Schematic diagrams of DNS contraction triggered by H1. (B) AFM image of DNS and the cross-section profile of the white line. (C)PAGE characterization of H-DNS synthesis and its conversion to DSC. Lane1: DSC; Lane2: H1; Lane3: H2; Lane4: H-DNS; Lane5: H-DNS and H1 mixture; Lane6: hybridized duplex H1/H2; Lane7: DNA ladder. (D) Schematic illustration and (E) PAGE characterization for in vitro verification of safety catch "on/off" status conversion and subsequent reaction with RL-RC. Lane1: DNA ladder; Lane2,7: MH, RC; Lane3–6,10: MH/RM, Pl/PC, MH/RM/PC, RL/RC, Pl/RL after annealed at 95 °C for 5 min and naturally cooled to room temperature; Lane8–9: mixture of MH/Pl-PC/RL-RC; mixture of MH/RM/Pl-PC/RL-RC at 37 °C for 30 min. (F) Fluorescence spectra of Pl-RL$_{F/T}$, mixture of MH/Pl-PC$_{F/D}$/RL$_T$-RC, the mixture of MH/RM/Pl-PC$_{F/D}$/RL$_T$-RC, the mixture of RL$_T$-RC/Pl$_F$ at λex of 488 nm. FAM emission peak is at 500–540 nm, and TRAMRA emission peak is at 560–620 nm. DNS: DNA nanostring, DSC: DNA scaffold. Pl-PC is the simplified version of safety catch PL-PC, RM is the simplified version of c-Met, MH-RM is the simplified version of MH binding to c-Met, RL-RC is the simplified version of SRL-RC, which reacts with Pl ("safety off" status of safety catch). The safety catch conversion process is simplified by incubating MH, RM with Pl-PC, which produces Pl as an indication of "safety off" status for safety catch. The DNS anchoring process is simplified by incubating Pl with RL-RC, which produces Pl-RL as an indication of DNS binding with safety catch. Uncropped images of gels for (C) and (E) are shown in Figure S30.

$_B$). Reacting with H1 detached H2 from H-DNS$_{T/B}$ and converted it to DSC$_{T/B}$, which significantly decreased TAMRA fluorescence (Figure S2B, +H1). The reversible TAMRA fluorescence recovery/quenching in response to alternate reactions with H2 and H1 confirmed the structure change of H-DNS during reaction process.

To estimate the repeating number of stretchable regions in DSC, S1$_T$/S3$_B$ couple was continuously added into DSC from very low concentration. S1$_T$ that hybridized to DSC showed very little fluorescence due to the proximate location of S3$_B$. After the anchoring positions in DSC were saturated, the continuous addition of S1$_T$/S3$_B$ resulted in free distributed S1$_T$ in reaction mixture and showed significant TAMRA fluorescence that increased with S1$_T$/S3$_B$ concentration (Figure S2C). By studying fluorescence curve inflection points, the number of repeating regions in DSC was determined as ~275 with estimated DNS length of ~6200 nm.

In vitro Verification of Safety Catch Status Conversions and DNS Anchoring

Duplex DNA strand PL-PC, as the safety catch that anchored to PD–L1, was prepared via hybridizing DNA strand PL with DNA strand PC. The DNS recognition region in PL was sealed via hybridization with PC (Scheme 1A, Safety catch PL-PC). To simplify experiment process for in vitro verification, Pl, the DNS recognition region in PL, was used instead of PL to hybridize with PC and obtained Pl-PC (Figure 1D, Pl-PC), which showed a

clear band on PAGE (Figure S3A, lane 7). A hairpin structured DNA MH recognized c-Met to expose PC hybridization region for initiating status conversion of safety catch (Scheme 1A, Cancer cell, "safety on", "safety off"). To simplify experiment process for in vitro verification, DNA strand RM, which has the complementary sequence to the c-Met recognition region in MH, was incubated with MH to represent c-Met/MH recognition. The as-obtained MH-RM has exposed PC recognition region (Figure 1D, MH-RM), which reacted with safety catch Pl-PC via a strand displacement reaction to convert it to "safety off" status (Pl) with the production of MH-RM-PC conjugate (Figure 1D, Safety catch status conversion). The reaction process was in vitro verified via PAGE. Incubation of MH and RM generated a new band with lower mobility on PAGE, indicating the successful generation of MH-RM (Figure S3A, lane 4). MH-RM was continuously incubated with the above-obtained Pl-PC, and clearly showed MH-RM-PC band with lower mobility and Pl band with higher mobility, in accompany with the complete disappearance of MH-RM band and Pl-PC band (Figure S3A, lane 9). On the contrary, MH didn't react with Pl-PC in the absence of RM, and demonstrated their respective corresponding bands (Figure S3A, lane 8). Fluorescence spectroscopy was also performed to verify status conversion of safety catch Pl-PC. Self-quenched Pl-$PC_{F/D}$ was prepared by hybridizing Pl_{FAM} with PC_{Dabcyl} (Figure S3B), which demonstrated strong FAM fluorescence recovery when incubating with MH and RM (Figure S3B, Pl-$PC_{F/D}$ + MH + RM). On the contrary, incubating Pl-$PC_{F/D}$ with MH in the absence of RM barely caused FAM fluorescence recovery (Figure S3B, Pl-$PC_{F/D}$ + MH).

To verify the feasibility of DNS binding in vitro, duplex DNA RL-RC, representing anchor DNA SRL-RC of DNS, was incubated with above obtained Pl to simplify experiment process. Pl reacted with RL-RC via a toehold-mediated strand displacement reaction, which produced Pl-RL duplex structure and released free RC (Figure 1D). Incubating RL-RC with Pl generated two new bands, which were located at RC and Pl-RL corresponding positions respectively (Figure S4A, lane 9). In the absence of MH and RM pretreatment, Pl-PC remained at "safety on" status, and couldn't react with RL-RC, which demonstrated their individual bands upon mixture (Figure S4A, lane 8). To verify the feasibility of safety catch secured DNS anchoring, MH was co-incubated with RM, Pl-PC, and RL-RC, which yielded three new bands at corresponding positions of RC, Pl-RL, and by-product MH-RM-PC, while the reactant bands were completely disappeared (Figure 1E, lane 9). On the contrary, incubating MH with Pl-PC and RL-RC in the absence of RM only showed their respective bands (Figure 1E, lane 8). Fluorescence spectroscopy was also performed to confirm the reaction feasibility of MH, RM, Pl-PC, and RL-RC. RL_T-RC was prepared by hybridizing RC with TAMRA labeled RL, and incubated with MH, RM and self-quenched Pl-$PC_{F/D}$, which acted as the simplified version of successive reaction process at tumor cells including safety catch status conversion and DNS coupling. The reaction product Pl-$RL_{F/T}$ demonstrated efficient fluorescence resonance energy transfer (FRET) process between FAM and TAMRA under 488 nm excitation (Figure 1F, S4B, MH + RM + Pl-$PC_{F/D}$ + RL_T-RC). In the absence of DNA strand RM, incubating MH with Pl-$PC_{F/D}$ and RL_T-RC was performed as the simplified version of DNS reaction with "safety on" status of safety catch for normal cells. It only showed very weak FAM/TAMRA fluorescence (Figure 1F, S4B, MH + Pl-$PC_{F/D}$ + RL_T-RC).

Anchoring Safety Catch to Cell Membrane and "on/off" Status Conversion

Breast cancer cell 4T1 was chosen as the sample cancer cell to demonstrate the therapeutic effect of safety catch secured PD–L1 degradation, while mouse islet β cells and mouse normal breast cell HC11 cells, which overexpress PD–L1 in response to IFN-γ stimulation, were chosen as the normal cells to evaluate its "off-tumor" toxicity. To visualize the expression levels of PD–L1 and trigger protein c-Met, the three cell types were incubated with FAM-labelled PD–L1 aptamer and TAMRA-labelled c-Met aptamer. All three cell types showed high expression levels of PD–L1 (Figure S5, S6, FAM), while only 4T1 cells showed obvious c-Met expression with TAMRA fluorescence (Figure S5, S6, TAMRA), indicating the capability of c-Met as trigger protein for safety catch "on/off" status conversion.

To visualize the process of c-Met triggering safety catch status conversion, PL-PC_F and $MH_{C/DBCO}$ were prepared respectively by labeling FAM to DNA strand PC and Cy3/DBCO to DNA strand MH, and sequentially incubated with 4T1 cells. It demonstrated obvious FAM fluorescence around cell membrane, indicating efficient anchoring of safety catch on PD–L1 (Figure 2B, PL-PC_F). Upon recognizing c-Met, $MH_{C/DBCO}$ opened hairpin structure and exposed PC hybridization region, which acted as a key to convert safety catch from "safety on" status (PL-PC_F) to "safety off" status (PL) with the generation of MH-$PC_{F/C}$ (Figure 2A, Status conversion). MH-$PC_{F/C}$ brought FAM and Cy3 into proximity to generate Cy3 fluorescence via the FRET process (Figure 2B, $MH_{C/DBCO}$).

To visualize anchoring of DNS to 4T1 cell membrane, DNS was labelled with Cy5 and DBCO ($DNS_{Cy5/DBCO}$, Figure S7A) and incubated with the as-treated 4T1 cell. PL initiated a toehold-mediated strand displacement reaction with $S3RL_{DBCO}$-RC that anchored on DNS, which generated PL–$S3RL_{DBCO}$ duplex to anchor DNS on cell membrane (Figure 2A, DNS anchoring). The successful anchoring of DNS was confirmed by the appearance of Cy5 fluorescence at 4T1 cell membrane (Figure 2B, $DNS_{Cy5/DBCO}$). On the contrary, the safety catch PL-PC_F remained at "safety on" status in the absence of trigger DNA $MH_{C/DBCO}$, which prevented $DNS_{Cy5/DBCO}$ anchoring to cell membrane and only showed FAM fluorescence for 4T1 cells that were treated with PL-PC_F and $DNS_{Cy5/DBCO}$ (Figure S8A). Flow cytometry analysis results were consistent with the confocal imaging. Strong Cy3 and Cy5 fluorescence were observed for 4T1 cells that treated with PL-PC_F, $MH_{C/DBCO}$ and $DNS_{Cy5/DBCO}$ (Figure S9, + $DNS_{Cy5/DBCO}$), while only FAM

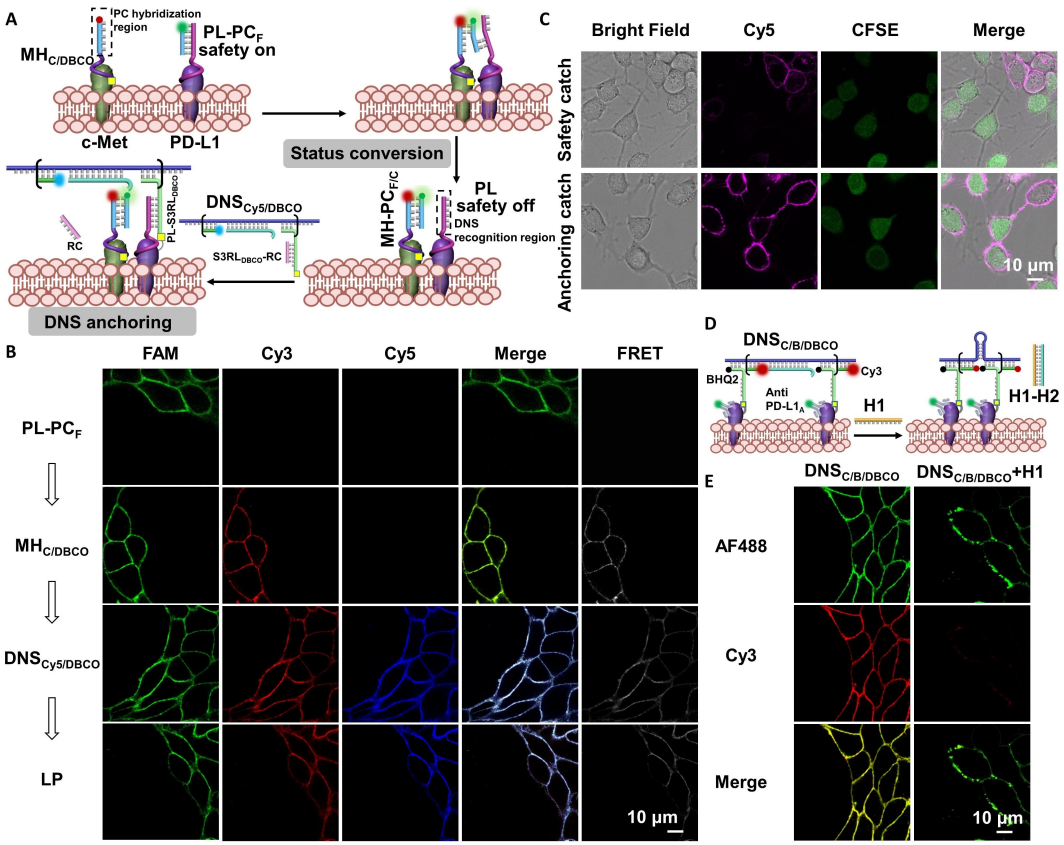

Figure 2. DNS anchoring on cell membrane and its contraction. (A) Schematic illustration of status conversion of safety catch and DNS anchoring. $MH_{C/DBCO}$ is MH labelled with Cy3 and DBCO, and PC_F is PC is labelled with FAM. PL-PC_F originally stays at "safety-on" status and shows FAM fluorescence. To convert safety catch to "safety-off" status, $MH_{C/DBCO}$ reacts with PL-PC_F, which results in FRET signal of TAMRA. $DNS_{Cy5/DBCO}$ is DNS labelled with Cy5 and DBCO. $DNS_{Cy5/DBCO}$ is then anchored by hybridizing with PL and shows Cy5 fluorescence on cell membrane. CLSM images of (B) 4T1 cells sequentially treated with PL-PC_F, $MH_{C/DBCO}$, $DNS_{Cy5/DBCO}$ and LP, (C) co-cultured 4T1 and HC11 cells treated with $DNS_{Cy5/DBCO}$. The co-cultured cells in "safety catch" group were pretreated with PL-PC and MH_{DBCO}, while the co-cultured cells in "anchoring catch" group were pretreated with PL. PL is the "safety off" status of PL-PC. By reacting with MH, safety catch PL-PC is converted to anchoring catch PL. 4T1 cells (c-Met positive) treated with PL-PC, MH_{DBCO} would convert safety catch to PL ("safety-off" status), $DNS_{Cy5/DBCO}$ is then anchored by hybridizing with PL and shows Cy5 fluorescence on cell membrane. HC11 cells (c-Met negative) treated with PL-PC_F, $MH_{C/DBCO}$, safety catch would stay at duplex ("safe on" status), $DNS_{Cy5/DBCO}$ is unable to anchor to cell membrane, and shows little Cy5 fluorescence on cell membrane. Pretreating with PL that has exposed DNS recognition region shows Cy5 fluorescence from both cell types. (D) Schematic illustration of DNS contraction. (E) CLSM images of 4T1 cells incubated with $DNS_{C/B/DBCO}$ and LP ($DNS_{C/B/DBCO}$) or sequentially incubated with $DNS_{C/B/DBCO}$, LP and H1 ($DNS_{C/B/DBCO}$ +H1), all the cells were pretreated with PL-PC and MH_{DBCO}.

fluorescence was observed for 4T1 cells that treated with PL-PC_F and $DNS_{Cy5/DBCO}$ (Figure S8B, C, +$DNS_{Cy5/DBCO}$). These results indicated that DNS only anchored to PD–L1 with safety catch in "off" status. To further evaluate the "on/off" status conversion efficiency for PD–L1 anchored safety catch, PL_F was set as "anchoring catch" control. 4T1 cells were incubated with PL_F and $DNS_{Cy5/DBCO}$, which showed similar membrane Cy5 fluorescence intensity compared with 4T1 cells that treated with PL-PC_F, $MH_{C/DBCO}$ and $DNS_{Cy5/DBCO}$ (Figure S10). These results indicated the effective status conversion of safety catch as well as efficient anchoring of DNS to cell membrane.

To verify safety catch secured cancer cell-selective DNS anchoring, normal breast cell HC11 and islet ß with PD–L1 expression at cell membrane but in lack of c-Met expression were also incubated with PL-PC_F, $MH_{C/DBCO}$, and $DNS_{Cy5/DBCO}$. $MH_{C/DBCO}$ could not be retained on cell membrane due to the absence of c-Met expression, therefore safety catch PL-PC_F remained at "safety on" status and the as-treated cells only showed FAM fluorescence both for confocal imaging (Figure S11, S12, $DNS_{Cy5/DBCO}$) and flow cytometry analysis (Figure S13, S14, +$DNS_{Cy5/DBCO}$). Neither FRET signal of Cy3 nor Cy5 fluorescence from $DNS_{Cy5/DBCO}$ was observed, indicating DNS barely anchored to noncancer cells. To completely eliminate the interference of safety catch to normal cells functions, it is necessary to erase it from cell membrane. The eraser DNA strand LP was incubated with cells that functionalized with safety catch PL-PC_F. LP hybridized with PL-PC_F via a strand displacement reaction, which completely removed safety catch from cell membrane by forming PL-LP duplex (Scheme 1B, Normal cell). The erasing of safety catch from normal cell membrane eliminated its perturbation to PD–L1 intrinsic function for normal cells.[26] After incubating with eraser stand LP, FAM

fluorescence disappeared from both HC11 cells and islet ß cells (Figure S11, S12, LP; Figure S13, S14, +LP), indicating little interference from safety catch to normal cells. The contribution of safety catch to cancer cell-selective DNS anchoring was also verified in cancer cell and normal cell mixtures. 4T1 cells were co-incubated with mouse islet ß cells or HC11 cells respectively, and treated with PL-PC, MH_{DBCO} and $DNS_{Cy5/DBCO}$. HC11 cells were preincubated with CFSE dye to distinguish them from the 4T1 cells, while mouse islet ß cells were distinguished from 4T1 cells by cell morphology. Obvious Cy5 fluorescence was observed from 4T1 cells for both cell mixture groups, while neighboring mouse islet ß (Figure S15, Safety catch) or HC11 cells (Figure 2C, Safety catch) displayed little Cy5 fluorescence. To set an "anchoring catch" control, 4T1/HC11 cell mixtures and 4T1/mouse islet ß cell mixtures were treated with PL and $DNS_{Cy5/DBCO}$, and Cy5 fluorescence was indiscriminately observed from both cancer cells and noncancerous cells (Figure 2C, S15, Anchoring catch). These results indicated cell membrane safety catch could provide good cancer cell selectivity for DNS anchoring with little effect on neighing normal cells.

To fasten DNA strands on cell membrane and prevent their detachment during in vivo application, proximity-enhanced click chemistry was performed in accompany with recognition guided anchoring. All three cell lines were treated with Ac_4ManNAz for the metabolic labeling of azide on sialic acids at cell membrane. MH was also functionalized with DBCO. Ac_4ManNAz treatment resulted in efficient azide labelling on cell membrane (Figure S16) with little toxicity to as-treated cells (Figure S17). Recognition-guided binding of DNA strands is necessary for proximity-enhanced click chemistry. Therefore, only 4T1 cells that have membrane receptor c-Met showed Cy3 fluorescence from cell membrane when incubated with $MH_{C/DBCO}$ (Figure S18, 4T1). There is no nonspecific anchoring of MH to cell membrane in the absence of membrane receptor-based aptamer recognition, and $MH_{C/DBCO}$ incubating with azide functionalized HC11 cell didn't show Cy3 fluorescence from cell membrane (Figure S18, HC11). DNS was also synthesized with Cy5 labeled S1 and DBCO functionalized S3RL-RC ($DNS_{Cy5/DBCO}$, Figure S7A) to fasten it on 4T1 cell membrane. Therefore, incubating with eraser strand LP didn't influence DNS stay on cell membrane, and showed little Cy5 fluorescence decrease (Figure 2B, LP; Figure S9, +LP), further confirming the solid anchoring of DNS on cancer cell membrane.

DNS Contraction on Cell Membrane and PD-L1 Degradation

To visualize DNS contraction on cell membrane, $DNS_{C/B/DBCO}$ was prepared with $S1_{Cy3}$ and $S3RL_{BHQ2/DBCO}$-RC, $S1_{Cy3}$ strand was labeled with Cy3 at the 5' terminus, and $S3RL_{B/DBCO}$ strand was labeled with BHQ2 and DBCO at the 3′ and 5′ ends ($DNS_{C/B/DBCO}$, Figure S7B). The contraction of DNS would shrink the distance between Cy3 and BHQ2 with corresponding Cy3 fluorescence quenching. The as-obtained $DNS_{C/B/DBCO}$ was anchored to 4T1 cells via hybridization with DNS recognition region of PL and fastened via proximity-enhanced click chemistry. After incubating with eraser strand LP, $DNS_{C/B/DBCO}$ was still fastened on cell membrane. PD–L1 receptor was also labeled with Alexa Fluor 488(AF488) modified PD–L1 antibody (Anti $PD–L1_A$) (Figure 2D). The as-treated 4T1 cells clearly showed bright Cy3 fluorescence and AF488 fluorescence that were uniformly distributed on cell membrane (Figure 2E, $DNS_{C/B/DBCO}$). The contraction of DNS was then initiated on cell membrane upon the addition of H1, which dropped H2 off DNS via a strand displacement reaction, recovered the stretchable region of DNS to hairpin structure, and resulted in the contraction of DNS with PD–L1 aggregation (Figure 2D). DNS contraction pulled Cy3 and BHQ2 into proximate position and caused correspondingly substantial suppression of Cy3 fluorescence around cell membrane. AF488 fluorescence was also converted from a smooth line to disconnected segments (Figure 2E, $DNS_{C/B/DBCO}$ +H1), indicating efficient PD–L1 aggregation. The result from flow cytometric analysis also showed an obvious decrease of Cy3 fluorescence from cell membrane (Figure S19), which was consistent with the confocal imaging.

The clustering of membrane receptors would trigger their endocytosis and degradation via the lysosome pathway.[27] AF488 fluorescence from Anti $PD–L1_A$ was co-localized with lysosome dye to trace PD–L1 aggregation and endocytosis. AF488 fluorescence and lysosome dye were separated for 4T1 cells that were only treated with DNS_{DBCO} (Figure 3A, DNS_{DBCO}). Subsequent treatment with H1 resulted in a good overlap of AF488 signal and lysosomal dye (Figure 3A, DNS_{DBCO}+H1), indicating the endocytosis of PD–L1 into the lysosomes due to aggregation caused by DNS contraction.

Aggregation-induced PD–L1 degradation efficiency was then evaluated by measuring PD–L1 expression levels on cell membranes via immunofluorescence, flow cytometry, and western blotting analysis. PD–L1 on cell membrane was labeled with Anti $PD–L1_A$, and membrane AF488 fluorescence was measured via confocal microscopy and flow cytometry. Azide functionalized 4T1, HC11, and islet ß cells were treated with 1) PL-PC; 2) MH_{DBCO}; 3) PL-PC/MH_{DBCO}; 4) PL respectively, followed by incubating with DNS_{DBCO} and H1/LP. Only the assembly of safety catch PL-PC didn't affect PD–L1 expression level for all the tested cell lines, since the safety catch remained at "safety-on" status in the absence of trigger strand MH_{DBCO} (Figure 3B, PL-PC). Only MH_{DBCO} treatment didn't affect PD–L1 expression either, since DNS_{DBCO} couldn't anchor on cell membrane in the absence of safety catch assembly (Figure 3B, MH_{DBCO}). Co-incubation with PL-PC and MH_{DBCO} converted the PL-PC safety catch to "safety off" status for cancer cells 4T1, which significantly suppressed PD–L1 expression and correspondingly showed a strong decrease of AF488 fluorescence on cell membrane (Figure 3B, 4T1, PL-PC+MH_{DBCO}). On the contrary, normal cells HC11 and islet ß barely showed AF488 fluorescence decrease compared with untreated groups (Figure 3B, Islet β, HC11, PL-PC+MH_{DBCO}), indicating safety catch can effectively protect

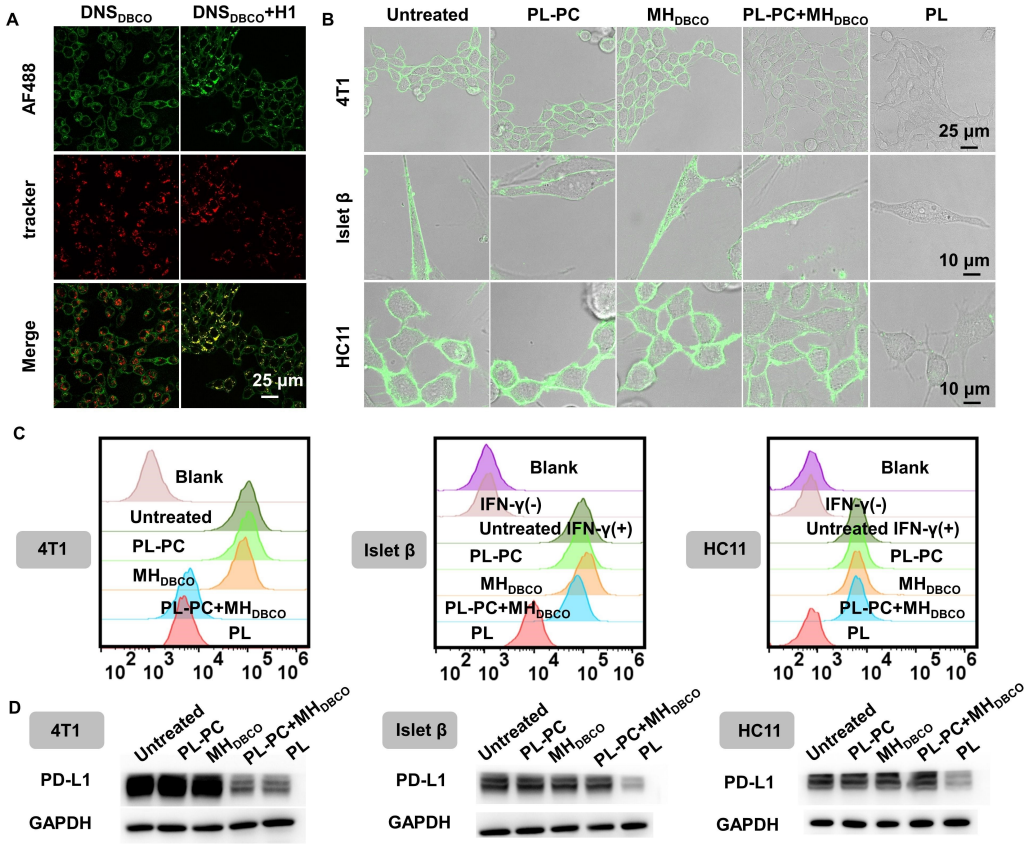

Figure 3. Characterization of PD–L1 degradation. CLSM images of (A) lysosome colocalization with PD–L1 for 4T1 cells treated with DNS_{DBCO} and LP or DNS_{DBCO} and H1/LP respectively. 4T1 cells in both groups were pretreated with PL-PC and MH_{DBCO}. (B) Immunofluorescence, (C)flow cytometry and (D) western blotting analysis of PD–L1 expressions for 4T1 cells, islet β cells, and HC11 cells that pretreated with PL-PC, MH_{DBCO}, PL-PC/MH_{DBCO}, and PL respectively with continuous incubation with DNS_{DBCO} and H1/LP, and the green channel with λex = 488 nm representing the signal of Anti PD–$L1_A$. Anti PD–$L1_A$ is the abbreviation of Alexa Fluor 488(AF488) modified PD–L1 antibody, and PL is the status that safety catch exposes the DNS recognition region and thus is available for DNS connection. Uncropped images of blots for (D) are shown in Figure S32A.

PD–L1 on noncancerous cells from degradation. These results demonstrated the capability of membrane safety catch for cancer cell-selective PD–L1 degradation. DNA strand PL, which directly hybridizes with SRL-RC for DNS_{DBCO} anchoring, was also incubated with three cell lines as the "anchoring catch" control. With the exposed DNS recognition region, PL could not discriminate cancer cells with noncancerous cells, which showed similar extent of AF488 fluorescence decrease for 4T1 cells compared with PL-PC/MH_{DBCO} treatment group (Figure 3B, 4T1, PL) and substantial AF488 fluorescence decrease for noncancerous cells HC11 and islet ß compared with PL-PC/MH_{DBCO} treatment group (Figure 3B, Islet β, HC11, PL). In lack of PC hybridization to seal DNS recognition region, PL couldn't discriminate cancer cells from normal cells, and showed "off-tumor" toxicity by degrading PD–L1 for both cancer cells and normal cells. To confirm that PD–L1 degradation was achieved via the lysosomal pathway, E-64, an irreversible and highly selective cysteine protease inhibitor that blocks protein degradation capability of lysosomes,[28] was pretreated with 4T1 cells. The as-treated 4T1 cells were incubated with PL-PC/MH_{DBCO}, DNS_{DBCO} and H1/LP, which showed no decrease of AF488 fluorescence on cell membrane compared with untreated cells (Figure S20A, PL-PC + MH_{DBCO}). These results indicated E-64 significantly impaired PD–L1 degradation efficiency, therefore confirmed the important role of lysosomes in PD–L1 degradation.

Flow cytometry analysis demonstrated similar results to confocal imaging. PL-PC/MH_{DBCO} pretreated 4T1 cells showed much lower AF488 fluorescence compared with untreated 4T1 cells and 4T1 cells that only treated with PL-PC or MH_{DBCO} (Figure 3C, 4T1), while PL-PC/MH_{DBCO} pretreated islet β cells (Figure 3C, Islet ß) and HC11 cells (Figure 3C, HC11) barely showed a fluorescence decrease compared with untreated controls. The "anchoring catch" control PL indiscriminately degraded PD–L1 for both cancer cells and noncancerous cells, and decreased fluorescence for all the treated cell types (Figure 3C, PL). western blotting analysis also showed effective degradation of PD–L1 for PL-PC/MH_{DBCO} pretreated 4T1 cells, while didn't affect PD–L1 degradation for PL-PC/MH_{DBCO} pretreated islet β cells and HC11 cells (Figure 3D, PL-PC + MH_{DBCO}). On the contrary, PL pretreatment showed PD–L1 degradation for 4T1 cells, islet β cells, and HC11 cells (Figure 3D, PL). While for 4T1 cells treated with protease

inhibitor E-64, PD–L1 expression (Figure S20B) and AF488 fluorescence signal (Figure S20C) were unchanged for all the pretreated groups compared with untreated cells. These results further confirmed that assembling safety catch could provide satisfactory cancer cell-selective PD–L1 degradation via lysosome pathway.

Evaluation of T Cell-Dependent Toxicity to Safety Catch Anchored Cells

Selective suppression of PD–L1 expression for cancer cells can effectively boost T cell antitumor toxicity. To evaluate the contribution of PD–L1 suppression to immunotherapy at the cellular level, azide labelled-4T1 cells were pretreated with PL-PC, MH_{DBCO}, PL-PC/MH_{DBCO}, and PL respectively, subsequently incubated with DNS_{DBCO} and H1/LP, and co-cultured with activated mouse peripheral blood mononuclear cells (aPBMCs) (labeled with CFSE dye as indicator) for 12 hours (Figure 4A). T cell-dependent toxicity was evaluated by observing the distributions of 4T1 cells and T cells. When incubating with 4T1 cells that were only pretreated with PL-PC or MH_{DBCO}, aPBMC cells were mainly located at the "vacant" places where 4T1 unseeded (as indicated by the red dash line) and barely penetrated to 4T1 cell proximity (Figure 4B, PL-PC, MH_{DBCO}). By inhibiting the immune checkpoint pathway with PD–L1 degradation, the immune escape of tumor cells is effectively suppressed.[29] Therefore, aPBMCs efficiently penetrated into the seeded 4T1 cells that were pretreated with PL-PC/MH_{DBCO}, and showed subsequently enhanced quantity around 4T1 cells (Figure 4B, PL-PC + MH_{DBCO}). These results indicated PD–L1 degradation effectively improved T cell recognition and killing capability. 4T1 cells that were pretreated with "anchoring catch" PL also showed similar density of aPBMCs around 4T1 cells compared with PL-PC/MH_{DBCO} pretreatment. The tendencies of T cell killing capability to 4T1 cells with different pretreatments were consistent with that of PD–L1 degradation levels. T cell-dependent toxicity was further evaluated by detecting cytokines IFN-γ and TNF-α secretions in the supernatant of 4T1 cells and aPBMCs co-culture. When incubating with PL-PC/MH_{DBCO} pretreated 4T1 cells, aPBMCs showed significantly enhanced secretion levels of IFN-γ (Figure 4C, PL-PC + MH_{DBCO}) and TNF-α (Figure 4D, PL-PC + MH_{DBCO}) compared with cytokine secretions when incubat-

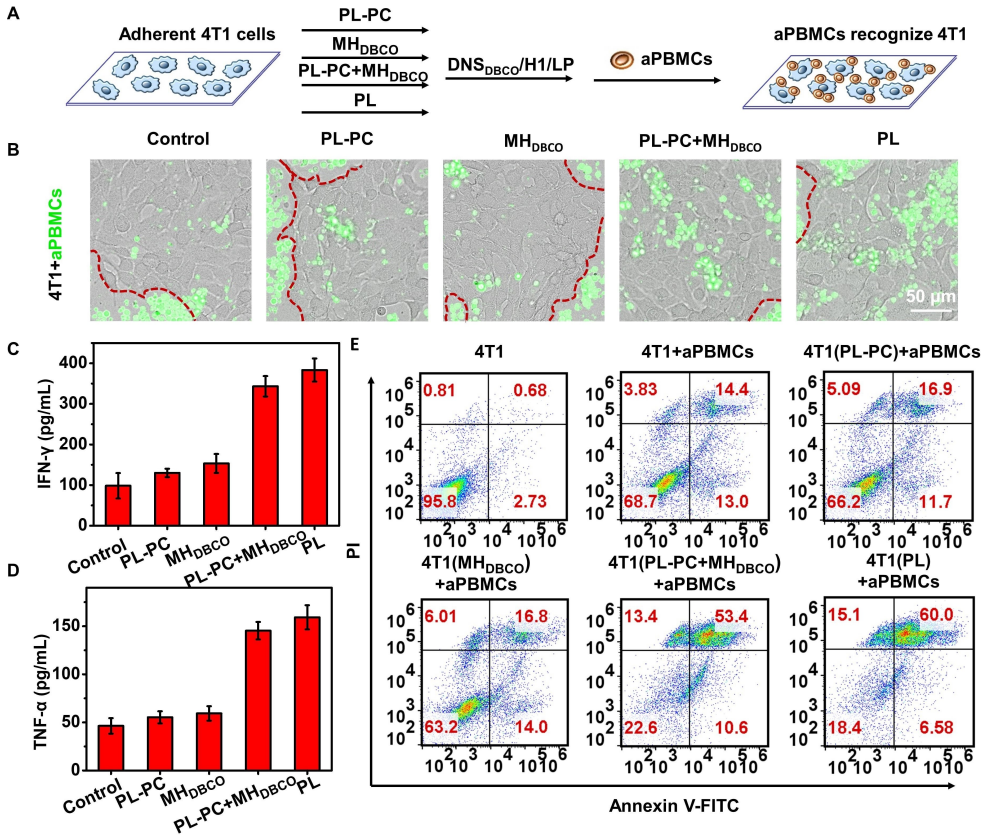

Figure 4. Effect of PD–L1 degradation on cytotoxicity in immune cells. (A) Schematic diagram for the experimental procedures of 4T1 cells co-incubated with aPBMCs. (B) CLSM of different processes pretreated 4T1 cells co-cultured with CFSE-stained aPBMCs for 12 h. (C) IFN-γ and (D) TNF-α levels in the supernatants of aPBMCs co-cultured with 4T1 cells with different pretreatment processes. (E) Apoptosis analysis of different processes pretreated 4T1 cells co-cultured with aPBMCs. Apoptosis or necrosis was determined by flow cytometry using Annexin V-FITC and PI staining. E/T ratio of 10:1. aPBMCs are activated mouse peripheral blood mononuclear cells, H1 contracts DNS_{DBCO}, PL is the status that safety catch exposes the DNS recognition region and thus is available for DNS connection, and LP is the eraser strand used to remove safety catch.

ing aPBMCs with 4T1 cells that merely pretreated with PL-PC or MH_{DBCO} (Figure 4C, 4D, PL-PC, MH_{DBCO}). Incubating aPBMCs with 4T1 cells that were pretreated with "anchoring catch" PL showed similar cytokine secretion levels compared with PL-PC/MH_{DBCO} pretreated 4T1 cells (Figure 4C, 4D, PL). These results indicated PD–L1 degradation at cancer cell membrane could effectively promote T cell activation.

The as-treated 4T1 cells were then stained with Annexin V-FITC/PI for flow cytometry analysis of cell apoptosis or necrosis induced by T cell killing. Compared with untreated 4T1 cells (Figure 4E, 4T1), co-incubation with aPBMCs resulted in 31.3 % of cell damage due to T cell toxicity (Figure 4E, 4T1 + aPBMCs). Pretreatment with PL-PC or MH_{DBCO} had very limited contributions to enhance T cell toxicity, which enhanced cell damage rates to 33.8 % (Figure 4E, 4T1(PL-PC) + aPBMCs) and 36.7 % (Figure 4E, 4T1(MH_{DBCO}) + aPBMCs), respectively. Pretreatment with PL-PC/MH_{DBCO} greatly enhanced T cell killing capability with cell damage rate of 77.4 % (Figure 4E, 4T1(PL-PC + MH_{DBCO}) + aPBMCs), which was similar to "anchoring catch" PL pretreatment (cell damage rate of 81.6 %) (Figure 4E, 4T1(PL) + aPBMCs). To confirm that the installing of safety catch on PD–L1 could provide satisfactory selectivity to guide T cell killing, azide-labeled mouse pancreatic islet β cells and normal breast HC11 cells were also pretreated with PL-PC, MH_{DBCO}, PL-PC/MH_{DBCO}, and PL respectively, subsequently incubated with DNS_{DBCO} and H1/LP, and then co-incubated with aPBMCs. Installing PD–L1 with safety catch PL-PC successfully prevented the systematic toxicity from unselective PD–L1 degradation, and demonstrated 20.5 % of cell damage for islet β cells (Figure S21, Islet β(PL-PC + MH_{DBCO}) + aPBMCs) and 23.9 % of cell damage for HC11 cells (Figure S22, HC11(PL-PC + MH_{DBCO}) + aPBMCs). On the contrary, pretreatment with "anchoring catch" PL could not discriminate cancer cells from normal cells for T cell killing, and showed a much higher cell damage rate of 56.3 % and 55.5 % for islet β cells (Figure S21, Islet β(PL) + aPBMCs) and HC11 cells (Figure S22, HC11(PL) + aPBMCs) respectively. The above results further confirmed the feasibility of safety catch-secured PD–L1 degradation to provide cancer cell-selective toxicity in immunotherapy.

In vivo Application of Cancer Cell-Selective PD-L1 Degradation to Immunotherapy

Phosphorothioate-modified safety catch PL-PC_{PT}, DNA strands MH_{PT}, SRL-RC_{PT} and DNS_{PT} were used for in vivo application to resist nuclease degradation.[30] The serum stability of Pl-PC_{PT}, MH_{PT}, RL-RC_{PT} and Pl-RL_{PT} was confirmed by PAGE analysis (Figure S23) and serum/nuclease stability of DNS_{PT} was confirmed by PAGE analysis and measuring fluorescence recovery of self-quenched DNS_{PT} ($DNS_{PT/T/B}$) (Figure S24). BALB/c mice bearing 4T1 tumors were used to evaluate the in vivo application of safety catch-secured PD–L1 degradation. To achieve efficient immunotherapeutic effect, it is necessary to activate T cells in vivo for immune killing. Therefore, chemotherapeutic drug DOX was administered by intratumoral injection, which induced immunogenic cell death and produced corresponding antigen that was processed and presented by dendritic cells to activate T cells.[31]

After Ac_4ManNAz and DOX administration, PL-PC_{PT}, $MH_{PT/DBCO}$ were sequentially administrated, the mice groups that administrated with 1) DOX, 2) DOX/PL-PC_{PT}; and 3) DOX/$MH_{PT/DBCO}$ were set as controls. All mice groups were also subsequently administrated with $DNS_{PT/DBCO}$ and $H1_{PT}$/LP_{PT}. $DNS_{PT/DBCO}$ was labeled with Cy5 to trace its distribution in vivo ($DNS_{PT/Cy5/DBCO}$, Figure S7C). The trigger DNA $MH_{PT/DBCO}$ successfully set safety catch in "safety off" status and demonstrated efficient gathering of $DNS_{PT/Cy5/DBCO}$ at tumor position (Figure S25, DOX + PL-PC_{PT} + $MH_{PT/DBCO}$). On the contrary, the safety catch remained in "safety-on" status for the control group that administrated with PL-PC_{PT} in the absence of $MH_{PT/DBCO}$, which could not retain $DNS_{PT/Cy5}/_{DBCO}$ at tumor position and barely showed fluorescence at tumor position (Figure S25, DOX + PL-PC_{PT}). $DNS_{PT/Cy5/BHQ3/DBCO}$ was prepared with $S1_{PT/Cy5}$ and S3$RL_{PT/BHQ3/DBCO}$-RC_{PT}, $S1_{PT/Cy5}$ strand was labeled with Cy5 at the 5' terminus, and S3$RL_{PT/BHQ3/DBCO}$-RC_{PT} strand was labeled with BHQ3 and DBCO at the 3′ and 5′ ends ($DNS_{PT/Cy5/BHQ3/DBCO}$, Figure S7D). The contraction of DNS would shrink the distance between Cy5 and BHQ3 with corresponding Cy5 fluorescence quenching. After the administration of PL-PC_{PT}, $MH_{PT/DBCO}$ and $DNS_{PT/Cy5/BHQ3/DBCO}$, Cy5 fluorescence was clearly observed at tumor site (Figure 5A, Before H1), indicating the efficient anchoring of DNS on tumor cells. The additional injection of $H1_{PT}$ significantly reduced Cy5 fluorescence at tumor position (Figure 5A, After H1), indicating efficient contraction of DNS in vivo.

In vivo contraction of DNS resulted in aggregation of PD–L1 and corresponding degradation, which would facilitate T-cell recognition of tumor cells to enhance immunotherapeutic effect. T cell distribution at tumor position was evaluated via immunohistochemical staining by staining tumor sections with Cy3 labeled CD4 antibody and FITC labeled CD8 antibody. Though the immunogenic death due to DOX administration recruited $CD8^+$ T cells to tumor position to some extent, the over-expressed PD–L1 at cancer cell membrane impaired immunotherapeutic efficiency for the control groups (Figure 5B, DOX, DOX + PL-PC_{PT}, DOX + $MH_{PT/DBCO}$). Pretreating with DOX/PL-PC_{PT}/$MH_{PT/DBCO}$ effectively degraded PD–L1 at cancer cell membrane after administration of DNS_{PT}/$H1_{PT}$, and significantly promoted $CD8^+$ T cell infiltration at tumor position (Figure 5B, DOX + PL-PC_{PT} + $MH_{PT/DBCO}$). Flow cytometry analysis was further performed to confirm the promotion of $CD8^+$ T cells distribution via PD–L1 degradation. The tumor tissue was dissected and homogenized into cell suspensions, and labeled with anti-CD3-PE, anti-CD8-FITC and anti-CD4-APC. Flow cytometry analysis demonstrated a similar tendency as immunohistochemical staining results. DOX, DOX/PL-PC_{PT} and DOX/$MH_{PT/DBCO}$ pretreatment groups showed around 25 % of $CD8^+$ T cell distributions due to the immunogenic death caused by DOX administration (Figure 5C, DOX, DOX + PL-PC_{PT}, DOX + $MH_{PT/}$

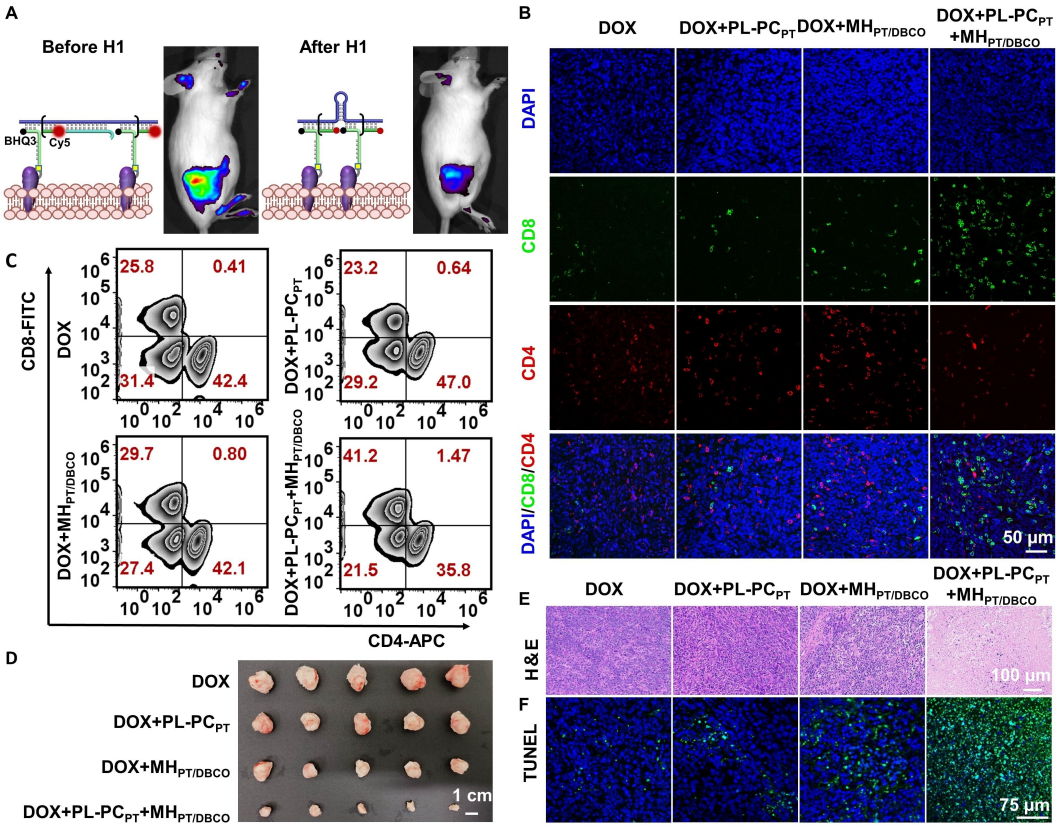

Figure 5. In vivo antitumor effects of safety catch secured cancer cell-selective PD–L1 degradation. (A) In vivo fluorescence imaging of PL-PC$_{PT}$/MH$_{PT/DBCO}$/DNS$_{PT/Cy5/BHQ3/DBCO}$ administrated mice groups before and after H1$_{PT}$/LP$_{PT}$ injection. (B) Representative immunofluorescence staining of tumor tissue infiltrated by immune cells. Blue, DAPI-labeled nuclei; red, CD4 antibody-labeled T cells; green, CD8 antibody-labeled T cells. (C) Flow cytometry plots showing the percentage of CD8$^+$ T cells among the CD3$^+$ cells in the tumors; (D) photographs of dissected 4T1 mice tumors; (E) H&E staining and (F)TUNEL staining of 4T1 tumors for DOX, DOX/PL-PC$_{PT}$, DOX/MHP$_{T/DBCO}$, DOX/PL-PC$_{PT}$/MH$_{PT/DBCO}$ pretreated mice groups. All the experiment groups were pretreated with DOX, "DOX + PL-PC$_{PT}$" indicates pre-incubation with safety catch PL-PC$_{PT}$, "DOX + MH$_{PT/DBCO}$" indicates pre-incubation with c-Met binding probe MH, and "DOX + PL-PC$_{PT}$ + MH$_{PT/DBCO}$" indicates pre-incubation with PL-PC$_{PT}$ and MH$_{PT/DBCO}$. The subscript PT indicates phosphorothioate-modified DNA strands.

$_{DBCO}$). DOX/PL-PC$_{PT}$/MH$_{PT/DBCO}$ pretreatment group obviously enhanced CD8$^+$ T cell distribution to 41.2 % (Figure 5C, DOX + PL-PC$_{PT}$ + MH$_{PT/DBCO}$), these results confirmed that PD–L1 degradation at tumor cells could effectively promote CD8$^+$ T cell distribution in tumor position. In addition to distribution enhancement, PD–L1 degradation at cell membrane also contributes to immune cell activation. To evaluate the activation of systemic immune cells, cytokines IFN-γ and TNF-α expression levels were measured in mice blood, which demonstrated a remarkable increase for DOX/PL-PC$_{PT}$/MH$_{PT/DBCO}$ pretreated mice group compared with DOX, DOX/PL-PC$_{PT}$, and DOX/MH$_{PT/DBCO}$ pretreatment mice group (Figure S26). These results demonstrated that PD–L1 degradation could boost the killing power of T cells against tumor cells.

To verify the systematic toxicity of PD–L1 degradation, pancreas was chosen as the model organ considering the expression of PD–L1 at islet ß cell membrane, and the pancreas sections were obtained for immunohistochemical staining of T cell infiltration. Both CD4$^+$ and CD8$^+$ T cells express CD3$^+$ receptors, so Cy3-labeled CD3 antibody were selected for staining T cells, and anti-insulin-FITC for staining islet β cells. Pretreatments with DOX/PL-PC$_{PT}$, DOX/MH$_{PT/DBCO}$, and DOX/PL-PC$_{PT}$/MH$_{PT/DBCO}$ demonstrated little local distribution of CD3$^+$ T cells in pancreas, which were similar to DOX treated group (Figure S27). These results confirmed the good selectivity of PD–L1 degradation only to cancer cells, which provided satisfactory protection of normal organs from immune cell attacks.

The tumor volume and body weight of mice were measured every two days to evaluate the antitumor efficiency. The administration of DOX and combination with PD–L1 suppression resulted in significant tumor size reduction of ~66 % (Figure 5D, S28 A, DOX + PL-PC$_{PT}$ + MH$_{PT/DBCO}$), indicating the contribution of immune checkpoint protein degradation to tumor growth inhibition. The tumor size was only reduced by ~12 % and ~20 % respectively for mice groups that only pretreated with DOX/PL-PC$_{PT}$ in the absence of trigger DNA MH$_{PT/DBCO}$ (Figure 5D, S28 A, DOX + PL-PC$_{PT}$) and that only administrated with DOX/MH$_{PT/DBCO}$ in the absence of PL-PC$_{PT}$ (Figure 5D, S28 A, DOX + MH$_{PT/DBCO}$). The reason for a little more reduction of tumor volume in the DOX + MH$_{PT/DBCO}$ group was that MH$_{PT/DBCO}$ blocked the c-Met signaling pathway,

which affected the activity of tumor cells.[32] All results indicated the capability of membrane safety catch to perform cancer cell-selective PD–L1 degradation and corresponding immunotherapeutic effect. In addition, H&E and TUNEL stained images of mice tumor slices demonstrated a similar tendency with the most significant cell nuclei shrinkage and visible apoptosis of tumor cells for DOX/PL-PC_{PT}/$MH_{PT/DBCO}$ pretreated mice group (Figure 5E, F). All mice groups did not show a significant change in body weight and obvious pathological abnormalities of major organs during the experimental period (Figure S28B, S29), confirming the biosafety of administrated DNA structures.

Conclusion

In summary, we developed a "safety catch" refitting PD–L1 strategy for selectively degrading PD–L1 only for cancer cells while avoiding normal cells damage. A "safety catch" DNA duplex was designed and assembled on PD–L1 to block the binding of immune checkpoint blockade (ICB) reagent. The ICB reagent was a retractable DNA nanostring with repeating hairpin structural units, which contracted after binding to PD–L1, and correspondingly drove PD–L1 clustering and degradation via lysosome pathway. The status conversion of safety catch was triggered by membrane receptor c-Met that overexpressed on cancer cell membrane, which secured PD–L1 degradation selectively for cancer cells with little effect on normal cells, and demonstrated effective in vivo immunotherapeutic results. The as-reported cancer cell-selective activation safety catch could be used as an efficient and powerful tool for precise immunotherapy. For future clinic transition, the operation process could be optimized by integrating all functional DNA strands into one nanocarrier and sequentially releasing them for functionalization. In addition, PEG coating to the loading carrier could further help to prevent against nuclease degradation and extend systematic circulation.

Acknowledgements

We gratefully acknowledge the National Natural Science Foundation of China (22022405, 22374073, 21974064), Natural Science Foundation of Jiangsu Province for Distinguished Young Scholars (BK20200010), State Key Laboratory of Analytical Chemistry for Life Science (5431ZZXM2204, 5431ZZXM2307).

Conflict of Interest

The authors declare no conflict of interest.

Data Availability Statement

The data that support the findings of this study are available from the corresponding author upon reasonable request.

Keywords: PD–L1 · immune checkpoint degradation · DNA nanostring · c-Met · immunotherapy

[1] a) R. S. Riley, C. H. June, R. Langer, M. J. Mitchell, *Nat. Rev. Drug Discovery* **2019**, *18*, 175–196; b) W. J. Lesterhuis, J. B. A. G. Haanen, C. J. A. Punt, *Nat. Rev. Drug Discovery* **2011**, *10*, 591–600.

[2] a) E. A. Rozeman, C. U. Blank, *Nat. Med.* **2019**, *25*, 879–882; b) S. P. Kubli, T. Berger, D. V. Araujo, L. L. Siu, T. W. Mak, *Nat. Rev. Drug Discovery* **2021**, *20*, 899–919.

[3] a) S. Rafiq, O. O. Yeku, H. J. Jackson, T. J. Purdon, D. G. van Leeuwen, D. J. Drakes, M. Song, M. M. Miele, Z. Li, P. Wang, S. Yan, J. Xiang, X. Ma, V. E. Seshan, R. C. Hendrickson, C. Liu, R. J. Brentjens, *Nat. Biotechnol.* **2018**, *36*, 847–856; b) N. Roper, M. J. Velez, A. Chiappori, Y. S. Kim, J. S. Wei, S. Sindiri, N. Takahashi, D. Mulford, S. Kumar, K. Ylaya, C. Trindade, I. Manukyan, A.-L. Brown, J. B. Trepel, J.-M. Lee, S. Hewitt, J. Khan, A. Thomas, *Nat. Commun.* **2021**, *12*, 3880; c) W. Piao, L. Li, V. Saxena, J. Iyyathurai, R. Lakhan, Y. Zhang, I. T. Lape, C. Paluskievicz, K. L. Hippen, Y. Lee, E. Silverman, M. W. Shirkey, L. V. Riella, B. R. Blazar, J. S. Bromberg, *Nat. Commun.* **2022**, *13*, 2176.

[4] a) A. Ribas, J. D. Wolchok, *Science* **2018**, *359*, 1350–1355; b) P. Sharma, S. Goswami, D. Raychaudhuri, B. A. Siddiqui, P. Singh, A. Nagarajan, J. Liu, S. K. Subudhi, C. Poon, K. L. Gant, S. M. Herbrich, S. Anandhan, S. Islam, M. Amit, G. Anandappa, J. P. Allison, *Cell* **2023**, *186*, 1652–1669.

[5] a) H. K. Koblish, L. Wu, L.-C. S. Wang, P. C. C. Liu, R. Wynn, J. Rios-Doria, S. Spitz, H. Liu, A. Volgina, N. Zolotarjova, K. Kapilashrami, E. Behshad, M. Covington, Y.-O. Yang, J. Li, S. Diamond, M. Soloviev, K. O'Hayer, S. Rubin, C. Kanellopoulou, G. Yang, M. Rupar, D. DiMatteo, L. Lin, C. Stevens, Y. Zhang, P. Thekkat, R. Geschwindt, C. Marando, S. Yeleswaram, J. Jackson, P. Scherle, R. Huber, W. Yao, G. Hollis, *Cancer Dis.* **2022**, *12*, 1482–1499; b) H. Zhu, F. Bengsch, N. Svoronos, M. R. Rutkowski, B. G. Bitler, M. J. Allegrezza, Y. Yokoyama, A. V. Kossenkov, J. E. Bradner, J. R. Conejo-Garcia, R. Zhang, *Cell Rep.* **2016**, *16*, 2829–2837; c) V. Radhakrishnan, S. Banavali, S. Gupta, A. Kumar, C. D. Deshmukh, S. Nag, S. K. Beniwal, M. Gopichand, R. Naik, K. C. Lakshmaiah, D. Mandavia, M. Ramchandra, K. Prabhash, *Ann. Oncol.* **2019**, *30*, v494.

[6] a) Y. Sun, L. Mo, X. Hu, D. Yu, S. Xie, J. Li, Z. Zhao, X. Fang, M. Ye, L. Qiu, W. Tan, Y. Yang, *ACS Nano* **2022**, *16*, 21129–21138; b) Y. Guo, Q. Zhang, Q. Zhu, J. Gao, X. Zhu, H. Yu, Y. Li, C. Zhang, *Sci. Adv.* **2022**, *8*, eabn2941; c) Y. Wei, G. Qin, Z. Wang, C. Zhao, J. Ren, X. Qu, *ACS Nano* **2023**, *17*, 5808–5820.

[7] a) Y. Wu, L. Zhou, Y. Zou, Y. Zhang, M. Zhang, L. Xu, L. Zheng, W. He, K. Yu, T. Li, X. Zhang, Z. Chen, R. Zhang, P. Zhou, N. Zhang, L. Zheng, T. Kang, *Nat. Can.* **2023**, *4*, 382–400; b) C. Shi, Y. Wang, M. Wu, Y. Chen, F. Liu, Z. Shen, Y. Wang, S. Xie, Y. Shen, L. Sang, Z. Zhang, Z. Gao, L. Yang, L. Qu, Z. Yang, X. He, Y. Guo, C. Pan, J. Che, H. Ju, J. Liu, Z. Cai, Q. Yan, L. Yu, L. Wang, X. Dong, P. Xu, J. Shao, Y. Liu, X. Li, W. Wang, R. Zhou, T. Zhou, A. Lin, *Nat. Commun.* **2022**, *13*, 6951; c) H. Wang, H. Yao, C. Li, H. Shi, J. Lan, Z. Li, Y. Zhang, L. Liang, J.-Y. Fang, J. Xu, *Nat. Chem. Biol.* **2018**, *15*, 42–50.

[8] a) S. L. Topalian, J. M. Taube, R. A. Anders, D. M. Pardoll, *Nat. Rev. Cancer* **2016**, *16*, 275–287; b) A. Goodman, S. P. Patel, R. Kurzrock, *Nat. Rev. Clin. Oncol.* **2016**, *14*, 203–220; c) J. C. Hassel, *Lancet Oncol.* **2016**, *17*, 1471–1472; d) L. Gandhi, D. Rodríguez-Abreu, S. Gadgeel, E. Esteban, E. Felip, F. De Angelis, M. Domine, P. Clingan, M. J. Hochmair, S. F. Powell, S. Y. S. Cheng, H. G. Bischoff, N. Peled, F.

Grossi, R. R. Jennens, M. Reck, R. Hui, E. B. Garon, M. Boyer, B. Rubio-Viqueira, S. Novello, T. Kurata, J. E. Gray, J. Vida, Z. Wei, J. Yang, H. Raftopoulos, M. C. Pietanza, M. C. Garassino, *N. Engl. J. Med.* **2018**, *378*, 2078–2092; e) J. E. Rosenberg, J. Hoffman-Censits, T. Powles, M. S. van der Heijden, A. V. Balar, A. Necchi, N. Dawson, P. H. O'Donnell, A. Balmanoukian, Y. Loriot, S. Srinivas, M. M. Retz, P. Grivas, R. W. Joseph, M. D. Galsky, M. T. Fleming, D. P. Petrylak, J. L. Perez-Gracia, H. A. Burris, D. Castellano, C. Canil, J. Bellmunt, D. Bajorin, D. Nickles, R. Bourgon, G. M. Frampton, N. Cui, S. Mariathasan, O. Abidoye, G. D. Fine, R. Dreicer, *Lancet* **2016**, *387*, 1909–1920.

[9] a) S. K. Alsaiari, S. S. Qutub, S. Sun, W. Baslyman, M. Aldehaiman, M. Alyami, A. Almalik, R. Halwani, J. Merzaban, Z. Mao, N. M. Khashab, *Sci. Adv.* **2021**, *7*, eabe7174; b) Q. Fan, Z. Chen, C. Wang, Z. Liu, *Adv. Funct. Mater.* **2018**, *28*, 1802540; c) M. P. Lokugamage, C. D. Sago, Z. Gan, B. R. Krupczak, J. E. Dahlman, *Adv. Mater.* **2019**, *31*, 1902251; d) K. Hirabayashi, H. Du, Y. Xu, P. Shou, X. Zhou, G. Fucá, E. Landoni, C. Sun, Y. Chen, B. Savoldo, G. Dotti, *Nat. Can.* **2021**, *2*, 904–918; e) X. Zhang, J. Guo, Z. Zhou, K. Feng, H. Liu, Y. Ruan, R. Chen, Z. Liu, T. Zhang, L. Tang, X. Sun, *Chem. Biomed. Imaging* **2023**, DOI: 10.1021/cbmi.3c00098; f) J. Wu, J. Chen, Y. Feng, S. Zhang, L. Lin, Z. Guo, P. Sun, C. Xu, H. Tian, X. Chen, *Sci. Adv.* **2020**, *6*, eabc7828.

[10] a) M. Ramos-Casals, J. R. Brahmer, M. K. Callahan, A. Flores-Chávez, N. Keegan, M. A. Khamashta, O. Lambotte, X. Mariette, A. Prat, M. E. Suárez-Almazor, *Nat. Rev. Dis. Primers* **2020**, *6*, 38; b) S. Yan, Z. Luo, Z. Li, Y. Wang, J. Tao, C. Gong, X. Liu, *Angew. Chem. Int. Ed.* **2020**, *59*, 17332.

[11] a) G. J. Freeman, A. J. Long, Y. Iwai, K. Bourque, T. Chernova, H. Nishimura, L. J. Fitz, N. Malenkovich, T. Okazaki, M. C. Byrne, H. F. Horton, L. Fouser, L. Carter, V. Ling, M. R. Bowman, B. M. Carreno, M. Collins, C. R. Wood, T. Honjo, *J. Exp. Med.* **2000**, *192*, 1027–1034; b) K. M. Au, R. Tisch, A. Z. Wang, *ACS Nano* **2021**, *15*, 19990–20002.

[12] a) R. J. Sullivan, J. S. Weber, *Nat. Rev. Drug Discovery* **2021**, *21*, 495–508; b) I. Puzanov, A. Diab, K. Abdallah, C. O. Bingham, C. Brogdon, R. Dadu, L. Hamad, S. Kim, M. E. Lacouture, N. R. LeBoeuf, D. Lenihan, C. Onofrei, V. Shannon, R. Sharma, A. W. Silk, D. Skondra, M. E. Suarez-Almazor, Y. Wang, K. Wiley, H. L. Kaufman, M. S. Ernstoff, *J. Immunother. Cancer* **2017**, *5*, 95.

[13] C. Xu, Y.-P. Chen, X.-J. Du, J.-Q. Liu, C.-L. Huang, L. Chen, G.-Q. Zhou, W.-F. Li, Y.-P. Mao, C. Hsu, Q. Liu, A.-H. Lin, L.-L. Tang, Y. Sun, J. Ma, *BMJ* **2018**, *363*, k4226.

[14] M. Atkinson, A. J. Lansdown, *Best Pract. Res. Clin. Endocrinol. Metab.* **2022**, *36*, 101635.

[15] a) C. Boutros, A. Tarhini, E. Routier, O. Lambotte, F. L. Ladurie, F. Carbonnel, H. Izzeddine, A. Marabelle, S. Champiat, A. Berdelou, E. Lanoy, M. Texier, C. Libenciuc, A. M. M. Eggermont, J.-C. Soria, C. Mateus, C. Robert, *Nat. Rev. Clin. Oncol.* **2016**, *13*, 473–486; b) C. Li, S. Zhou, J. Chen, X. Jiang, *Chem. Biomed. Imaging* **2023**, *1*, 495–508.

[16] a) L. Li, Y. Li, C. H. Yang, D. C. Radford, J. Wang, M. Janát-Amsbury, J. Kopeček, J. Yang, *Adv. Funct. Mater.* **2020**, *30*, 1908961; b) S. Yang, M. K. Shim, S. Song, H. Cho, J. Choi, S. I. Jeon, W. J. Kim, W. Um, J. H. Park, H. Y. Yoon, K. Kim, *Biomaterials* **2022**, *290*, 121841.

[17] a) X. Liu, Y. Li, K. Wang, Y. Chen, M. Shi, X. Zhang, W. Pan, N. Li, B. Tang, *Nano Lett.* **2021**, *21*, 7862–7869; b) Z. Zhao, Y. Zhang, M. Wu, C. Yan, Z. Guo, *Chem. Biomed. Imaging* **2023**, *1*, 620–627.

[18] K. W. K. Lam, J. H. C. Chau, E. Y. Yu, F. Sun, J. W. Y. Lam, D. Ding, R. T. K. Kwok, J. Sun, X. He, B. Z. Tang, *ACS Nano* **2023**, *17*, 7145–7156.

[19] a) J. Dai, J. J. Hu, X. Dong, B. Chen, X. Dong, R. Liu, F. Xia, X. Lou, *Angew. Chem. Int. Ed.* **2022**, *61*, e202117798; b) Y. Wang, X. Li, D. Zheng, Y. Chen, Z. Zhang, Z. Yang, *Adv. Funct. Mater.* **2021**, *31*, 2102505.

[20] D. F. Quail, J. A. Joyce, *Nat. Med.* **2013**, *19*, 1423–1437.

[21] Y. Zhang, W. Chen, Y. Fang, X. Zhang, Y. Liu, H. Ju, *J. Am. Chem. Soc.* **2021**, *143*, 15233–15242.

[22] R. Guo, J. Luo, J. Chang, N. Rekhtman, M. Arcila, A. Drilon, *Nat. Rev. Clin. Oncol.* **2020**, *17*, 569–587.

[23] D.-Y. Oh, Y.-J. Bang, *Nat. Rev. Clin. Oncol.* **2019**, *17*, 33–48.

[24] T. Maurer, M. Eiber, M. Schwaiger, J. E. Gschwend, *Nat. Rev. Urol.* **2016**, *13*, 226.

[25] a) R. Deng, L. Tang, Q. Tian, Y. Wang, L. Lin, J. Li, *Angew. Chem. Int. Ed.* **2014**, *53*, 2389–2393; b) Y. Lv, R. Hu, G. Zhu, X. Zhang, L. Mei, Q. Liu, L. Qiu, C. Wu, W. Tan, *Nat. Protoc.* **2015**, *10*, 1508–1524.

[26] Y. Yang, J. Xu, Y. Sun, L. Mo, B. Liu, X. Pan, Z. Liu, W. Tan, *J. Am. Chem. Soc.* **2021**, *143*, 8391–8401.

[27] P. R. Moody, E. J. Sayers, J. P. Magnusson, C. Alexander, P. Borri, P. Watson, A. T. Jones, *Mol. Ther.* **2015**, *23*, 1888–1898.

[28] J. Qi, S. Jia, X. Kang, X. Wu, Y. Hong, K. Shan, X. Kong, Z. Wang, D. Ding, *Adv. Mater.* **2022**, *34*, 2203309.

[29] Y. Wu, C. Zhang, X. Liu, Z. He, B. Shan, Q. Zeng, Q. Zhao, H. Zhu, H. Liao, X. Cen, X. Xu, M. Zhang, T. Hou, Z. Wang, H. Yan, S. Yang, Y. Sun, Y. Chen, R. Wu, T. Xie, W. Chen, A. Najafov, S. Ying, H. Xia, *Nat. Commun.* **2021**, *12*, 2346.

[30] J. W. Taylor, W. Schmidt, R. Cosstick, A. Okruszek, F. Eckstein, *Nucleic Acid Ther.* **1985**, *13*, 8749–8764.

[31] a) G. Kroemer, L. Galluzzi, O. Kepp, L. Zitvogel, *Annu. Rev. Immunol.* **2013**, *31*, 51–72; b) J. Lu, X. Liu, Y.-P. Liao, F. Salazar, B. Sun, W. Jiang, C. H. Chang, J. Jiang, X. Wang, A. M. Wu, H. Meng, A. E. Nel, *Nat. Commun.* **2017**, *8*, 1811.

[32] a) R. Ueki, S. Atsuta, A. Ueki, S. Sando, *J. Am. Chem. Soc.* **2017**, *139*, 6554–6557; b) K. Chen, J. Cai, S. Wang, Y. Li, C. Yang, T. Fu, Z. Zhao, X. Zhang, W. Tan, *Angew. Chem. Int. Ed.* **2023**, *62*, e202208451.

Manuscript received: February 4, 2024
Accepted manuscript online: February 29, 2024
Version of record online: ■■, ■■

Research Articles

Immunotherapy

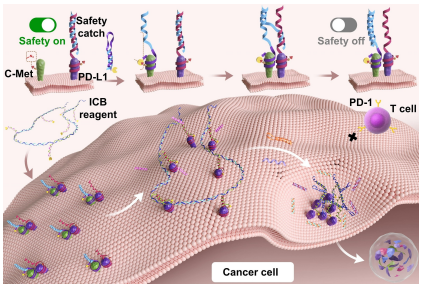

The "safety catch", a duplex DNA strand, was assembled on PD–L1 to control its accessibility by immune checkpoint blockade (ICB) reagent. ICB reagent was a retractable DNA nanostring (DNS), whose contraction drove PD–L1 clustering and corresponding degradation. 4T1 cell membrane protein c-Met controlled ICB reagent binding and achieved cancer cell selective PD–L1 inhibition. This strategy enhanced immunotherapeutic specificity.